

Tracing the Roots: Leveraging Temporal Dynamics in Diffusion Trajectories for Origin Attribution

Andreas Floros[†], Seyed-Mohsen Moosavi-Dezfooli^{‡,*}, Pier Luigi Dragotti[†]

[†]Imperial College London, [‡]Apple
{andreas.floros18, p.dragotti}@imperial.ac.uk, smoosavi@apple.com

Abstract

Diffusion models have revolutionized image synthesis, garnering significant research interest in recent years. Diffusion is an iterative algorithm in which samples are generated step-by-step, starting from pure noise. This process introduces the notion of diffusion trajectories, i.e., paths from the standard Gaussian distribution to the target image distribution. In this context, we study discriminative algorithms operating on these trajectories. Specifically, given a pre-trained diffusion model, we consider the problem of classifying images as part of the training dataset, generated by the model or originating from an external source. Our approach demonstrates the presence of patterns across steps that can be leveraged for classification. We also conduct ablation studies, which reveal that using higher-order gradient features to characterize the trajectories leads to significant performance gains and more robust algorithms.

1 Introduction

Generative modeling has seen major breakthroughs due to advances in Denoising Diffusion Probabilistic Models (DDPMs) (Sohl-Dickstein et al. 2015; Ho, Jain, and Abbeel 2020; Rombach et al. 2022). These models have become the go-to method for image synthesis, achieving state-of-the-art performance (Dhariwal and Nichol 2021; Karras et al. 2024). However, as diffusion models become more prevalent, concerns about privacy and security arise. With no one to hold the systems’ developers responsible, copyrighted or confidential data may be used in the training process and regurgitated during inference (Carlini et al. 2023; Somepalli et al. 2023; Wen et al. 2024; Gu et al. 2024). Moreover, the lack of accountability mechanisms enables the creation and dissemination of harmful or malicious content. Towards more responsible image generation, we develop algorithms to trace the origin of images.

In particular, we are interested in whether a given image is part of a model’s member (training) set, belonging set (i.e., sampled from the model) or if it is from an external dataset. Such problems are typically studied as two separate binary classification tasks in the literature. One task, membership inference, predicts whether a given image is part of a model’s member set (Shokri et al. 2017; Matsumoto, Miura, and Yanai 2023; Duan et al. 2023; Wang et al. 2024).

*Work done while at Imperial.

The second, Model Attribution (MA), aims to classify images as generated by a particular model (Wang et al. 2023; Laszkiewicz et al. 2024) (i.e., belonging to the model). We introduce the three-class problem of distinguishing member, belonging and external data as Origin Attribution (OA).¹

Focusing on the more common Membership Inference Attack (MIA) setting, existing methods typically train additional surrogate, or shadow, models (Shokri et al. 2017). In doing so, shadow models imitate the target model and can be used to estimate the classification boundary between members and non-members, without access to the target’s data. However, a limitation of such attacks is that it may not be feasible to produce these surrogates due to high computational costs and undocumented training processes (e.g., unknown training iterations, dataset size and regularization) (Dubiński et al. 2024). Also, shadow model training implicitly assumes knowledge of the member distribution, potentially leaking information, and fails to address distribution shifts (Das, Zhang, and Tramèr 2024; Dubiński et al. 2024). With these points in mind, we aim to develop practical, surrogate-free, attacks that make minimal assumptions about the data availability and training process of the diffusion model. Our contributions are three-fold:

- We simulate realistic attack environments for membership inference and evaluate existing attacks under this setting. Our results reveal two key problems with current approaches. Namely, threshold-based MIAs break down in the presence of belonging data and distribution shifts.
- We propose alternative algorithms that are shown to be more robust. Specifically, we tailor our methods to diffusion models and design attacks that leverage their multi-step nature. We present results for membership inference and extend our analysis to the MA and OA tasks.
- To better capture the multi-step dynamics of diffusion, we consider higher-order gradient features in combination with the commonly used loss features found in the literature. This feature space greatly improves the performance of our MIAs, MA and OA.

¹Note that Wang et al. (2023) use this term to describe what we call MA. However, we reserve the OA label for our more general setting and adopt MA to describe their setup, following Laszkiewicz et al. (2024).

2 Background

2.1 Diffusion-Based Generative Models

Continuous-time formulation. Diffusion models define a mapping between the data distribution, $p(\mathbf{x})$, and a normal distribution. Let $\mathbf{x}(\cdot) : [0, T] \rightarrow \mathcal{X}$, such that $\mathbf{x}(0) \sim p(\mathbf{x})$, and $\mathbf{x}(T)$ is normal. Diffusion from time $t = 0$ to $t = T$ can be modeled as the solution to an Itô Stochastic Differential Equation (SDE) (Song et al. 2021):

$$d\mathbf{x} = \mathbf{f}(\mathbf{x}, t)dt + g(t)d\mathbf{w}, \quad (1)$$

where $\mathbf{f}(\cdot, t) : \mathcal{X} \rightarrow \mathcal{X}$, $g(\cdot) : \mathbb{R} \rightarrow \mathbb{R}$ are appropriate drift, diffusion coefficients, and \mathbf{w} is the standard Wiener process. Sampling is performed from $t = T$ to $t = 0$ by modeling trajectories with a reverse-time SDE (Anderson 1982) as:

$$d\mathbf{x} = [\mathbf{f}(\mathbf{x}, t) - g(t)^2 \nabla_{\mathbf{x}} \log p_t(\mathbf{x})]dt + g(t)d\bar{\mathbf{w}}, \quad (2)$$

where $dt < 0$, and $\bar{\mathbf{w}}$ is the time-reversed standard Wiener process. Modeling the reverse diffusion trajectories requires knowledge of the score function $\nabla_{\mathbf{x}} \log p_t(\mathbf{x})$.

Denoising diffusion probabilistic models. In practice, one discretizes the above equations and considers families of SDEs with a tractable forward process. A common parameterization is given by DDPMs (Ho, Jain, and Abbeel 2020), which choose $\mathbf{f}(\mathbf{x}, t) = -\frac{1}{2}\beta(t)\mathbf{x}$ and $g(t) = \sqrt{\beta(t)}$, where the function $\beta(t)$ is the noise schedule. By discretizing (1) with DDPM, the forward probabilities become:

$$p_t(\mathbf{x}_t|\mathbf{x}) = \mathcal{N}(\mathbf{x}_t; \sqrt{\bar{\alpha}_t}\mathbf{x}, (1 - \bar{\alpha}_t)\mathbf{I}), \quad (3)$$

where the subscripts denote discretization, $\alpha_t = 1 - \beta_t$ and $\bar{\alpha}_t = \prod_{s=0}^t \alpha_s$. As $p_t(\mathbf{x}_t|\mathbf{x})$ is normal, the score is approximated by application of Tweedie’s formula (Efron 2011):

$$\nabla_{\mathbf{x}_t} \log p_t(\mathbf{x}_t) = \frac{\sqrt{\bar{\alpha}_t} \mathbb{E}(\mathbf{x}|\mathbf{x}_t, t) - \mathbf{x}_t}{1 - \bar{\alpha}_t}, \quad (4)$$

where the expectation describes the minimum Mean Squared Error (MSE) Gaussian denoiser. Therefore, score matching may be performed via a noise-predicting neural network, $\epsilon_{\theta}(\cdot, t) : \mathcal{X} \rightarrow \mathcal{X}$, such that it minimizes the quantity $\mathcal{L}_t = \|\epsilon_{\theta}(\sqrt{\bar{\alpha}_t}\mathbf{x} + \sqrt{1 - \bar{\alpha}_t}\epsilon, t) - \epsilon\|_2^2$. The complete DDPM minimization objective is then expressed as the following weighted average:

$$\min_{\theta} \mathbb{E}_{t \sim \mathcal{U}\{0, T-1\}, \mathbf{x} \sim p(\mathbf{x}), \epsilon \sim \mathcal{N}(\mathbf{0}, \mathbf{I})} \lambda_t \mathcal{L}_t. \quad (5)$$

For appropriate λ_t , the above is equivalent to the Negative Evidence Lower Bound (NELBO) of the data up to a constant (Ho, Jain, and Abbeel 2020). Thus, denoising score matching can be re-framed as likelihood maximization.

2.2 Data Forensics

Membership inference attacks. MIAs aim to determine whether a given sample is from the training set of a model. Formally, we are given a dataset, $\mathcal{D} = \mathcal{D}_M \cup \mathcal{D}_H$, and a model trained on \mathcal{D}_M . Here, \mathcal{D}_M refers to the member set, while \mathcal{D}_H denotes the hold-out set. The goal is to design, with limited data access, a classifier, y , such that:

$$y = \mathbf{1}[\mathbf{x} \in \mathcal{D}_M] = \begin{cases} 1 & \mathbf{x} \in \mathcal{D}_M \\ 0 & \text{otherwise} \end{cases}. \quad (6)$$

Since the model is optimized to minimize its loss on the training data, it is expected that \mathcal{D}_M achieves lower values than \mathcal{D}_H (Yeom et al. 2018). Based on this observation, Matsumoto, Miura, and Yanai (2023) develop an attack for diffusion models that assesses membership using the loss value at a given time-step, t , and a tunable threshold τ . Their classifiers take the following form:

$$y = \mathbf{1}[\mathcal{L}_t < \tau], \quad (7)$$

where t and τ are calibrated to maximize the attack’s effectiveness. Shadow models are often used for this purpose, i.e., models where their member set is known and that are produced solely for the purpose of mimicking the target model and tuning the attack (Shokri et al. 2017).

Observe that \mathcal{L}_t in (7) is stochastic as it depends on the noise $\epsilon \sim \mathcal{N}(\mathbf{0}, \mathbf{I})$. However, it is also possible to devise a deterministic scheme (Duan et al. 2023; Kong et al. 2024). Of note is the Proximal Initialization Attack (PIA) (Kong et al. 2024), which computes the following instead of \mathcal{L}_t :

$$\|\epsilon_{\theta}(\sqrt{\bar{\alpha}_t}\mathbf{x} + \sqrt{1 - \bar{\alpha}_t}\epsilon_{\theta}(\mathbf{x}, 0), t) - \epsilon_{\theta}(\mathbf{x}, 0)\|_p. \quad (8)$$

Alternative to the above threshold-based attacks, Pang et al. (2024) have also explored white-box attacks against diffusion models, where they train decision trees to classify features derived from Gradient Subsampling and Aggregation (GSA). In particular, they group the parameters of ϵ_{θ} and compute $\|\mathbb{E}_t \nabla_{\theta_i} \mathcal{L}_t\|_2^2$ or $\mathbb{E}_t \|\nabla_{\theta_i} \mathcal{L}_t\|_2^2$ with $\bigcup_i \theta_i = \theta$.

Synthetic data detection. Besides knowing whether a sample is part of the member set, we are interested in whether the sample was generated by a model. Intuitively, if we assume access to the models, this task is easier than blind synthetic data detection, and one can adapt the above MIAs for diffusion-generated image detection (Ma et al. 2023).

In another line of work, Wang et al. (2023) consider the harder MA task, where they stress the importance of attributing synthetic data to the specific generative model responsible for producing it. Wang et al. (2023) develop a general method based on the reconstruction loss. That is, a model able to synthesize the image in question from its latent space with minimal error is likely responsible for generating it.

3 Proposed Method

3.1 Motivation

In this paper, we consider the general problem of OA. Namely, we wish to simultaneously distinguish member, belonging and external data. A fitting scenario where our methods can be applied is as follows: An organization has released an open-weights, large diffusion model to the public. They have not disclosed what data was used to train the model or their training setup. However, a small fraction of training samples is available, either due to leaks or because one may assume that standard research datasets were included in the training set.

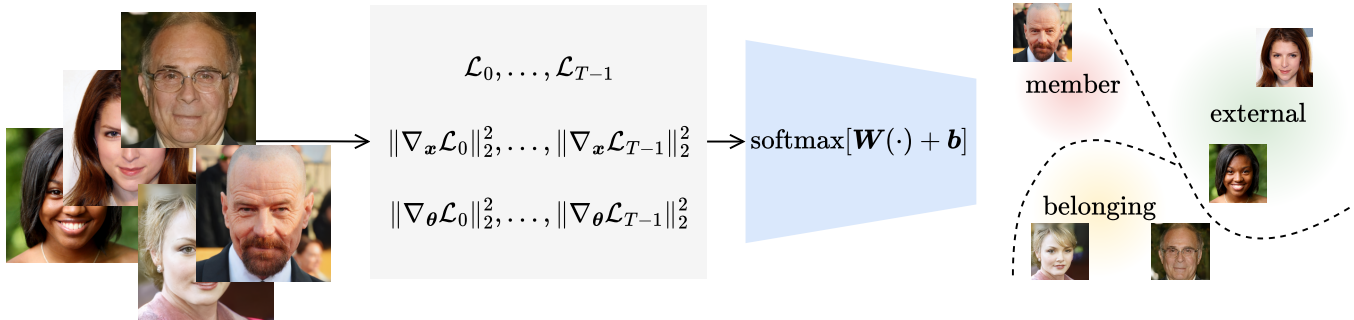


Figure 1: Overview of our method. Given an image, we model its diffusion trajectory by extracting and concatenating features at different time-steps. We then train linear algorithms on these representations to classify data as member, belonging or external.

Algorithm 1 Diffusion trajectory feature extraction

Input: Image x

Parameters: Trained DDPM, ϵ_θ , with schedule $\{\bar{\alpha}_t\}_{t=0}^{T-1}$

Output: Trajectory features f

```

1:  $f \leftarrow \{\}$ 
2: for  $t \in \{0, \dots, T-1\}$  do
3:    $\epsilon \sim \mathcal{N}(\mathbf{0}, \mathbf{I})$ 
4:    $\mathcal{L}_t \leftarrow \|\epsilon_\theta(\sqrt{\bar{\alpha}_t}x + \sqrt{1-\bar{\alpha}_t}\epsilon, t) - \epsilon\|_2^2$ 
5:    $f \leftarrow f \cup \{\mathcal{L}_t, \|\nabla_x \mathcal{L}_t\|_2^2, \|\nabla_\theta \mathcal{L}_t\|_2^2\}$ 
6: end for
7: return  $f$ 

```

We focus on two primary use cases of our OA framework that empower data owners to hold model developers accountable. First, given a non-belonging image, one can use OA to determine whether it is part of the member set. For example, an artist may want to confirm that their work was not used in the development of the model. Second, in case of belonging data, if one becomes suspicious of a particular generation, or they decide to use it as part of their own work, OA should ideally be able to test it for membership to ensure that it is not a result of the model memorizing and that there are no privacy and security violations.

As we will demonstrate below, existing MIAs are inflexible, since they are specifically engineered to operate on member and external data. Besides, with our setup, we additionally aim to capture the MA task, which further extends the utility of our methods. For instance, beyond addressing data rights, if the model produces harmful or malicious content, one could also use our attacks to verify that the content is fake and can be attributed (belongs) to the model.

3.2 Overview

Given a relevant image, x , we construct a feature vector, f , which is obtained from the diffusion models and x . We then produce logits, l , for classification as follows:

$$l = W \cdot f + b, \quad (9)$$

where W and b are learned based on a limited data budget. Our OA method, specifically, is detailed in Figure 1 and Algorithm 1. We provide further discussion below.

	Batch size	50
	Epochs	100
AdamW	Learning rate	1e-3
	Weight decay	10
StepLR	Step size	5 epochs
	Learning rate decay	0.8

Table 1: Classifier hyperparameters.

3.3 Characterization of Diffusion Trajectories

For an image, x , and a DDPM, ϵ_θ , we would like to develop a classifier that leverages the dynamics of diffusion and operates on the reverse trajectory of x , i.e., starting from $t = T$ and ending at $t = 0$. In practice, we can generate a forward trajectory sequence, $\{x_t\}_{t=0}^{T-1}$, for example, by application of (3).² Then, as the forward process is independent of ϵ_θ , we can introduce this dependency and simulate the reverse by discretizing (2) from t to $t-1$.

However, operating on the trajectories directly is intractable. For one, a typical diffusion sequence can contain hundreds of steps, and this suggests that extracting trajectories for processing may require hundreds of times more storage compared to the original data. For example, we estimate that trajectories of 1000 256×256 RGB images require roughly 786 GB at single-precision format for a DDPM with $T = 1000$. Additionally, training a classifier on such high-dimensional features would result in severe overfitting, given our assumption of limited data.

To simplify matters, we compress the diffusion trajectories into a lower-dimensional space by collapsing their spatial dimensions. We first consider a simple projection that produces the diffusion loss features $\{\mathcal{L}_t\}_{t=0}^{T-1}$. This choice of features naturally extends the single-step classification algorithms (Matsumoto, Miura, and Yanai 2023; Kong et al. 2024), which are described by (7), as thresholding is equivalent to one-dimensional linear classification with (9).

²Note that this trajectory sequence is not native to DDPMs. It corresponds to the forward process proposed by Huberman-Spiegelglas, Kulikov, and Michaeli (2024).

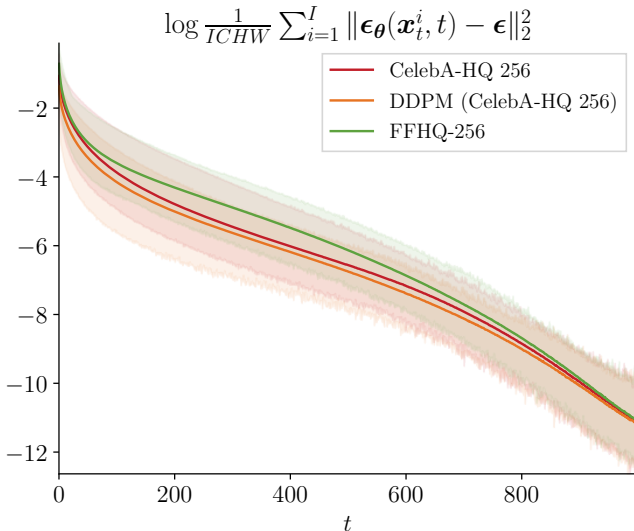


Figure 2: Average member, belonging and external data loss (solid lines) as a function of t for CelebA-HQ 256 DDPM.

Higher-order features. Pang et al. (2024) show that gradients, $\nabla_{\theta}\mathcal{L}_t$, can be used for MIAs and may outperform the loss features. In light of this, we include $\{\|\nabla_{\mathbf{x}}\mathcal{L}_t\|_2^2\}_{t=0}^{T-1}$ and $\{\|\nabla_{\theta}\mathcal{L}_t\|_2^2\}_{t=0}^{T-1}$ in our feature extraction pipeline. Intuitively, as the loss measures the score matching error, these higher-order features can be seen as a proxy for the Hessian of the likelihood of the data. We expect that this curvature information will be helpful in describing the trajectories.

4 Experiments

4.1 Setup

Datasets and generative models. We study DDPMs³ trained on CIFAR-10 (Krizhevsky 2009) and CelebA-HQ 256 (Karras et al. 2018), according to Ho, Jain, and Abbeel (2020), and use their recommended settings for sampling belonging data. For external data, we use CIFAR-10.1 (Recht et al. 2018; Torralba, Fergus, and Freeman 2008) and FFHQ-256 (Karras, Laine, and Aila 2018). We pick 1000 images (< 3.4% of member set) from each class for classifier training and evaluate on separate, similarly chosen datasets. For MA, we evaluate with non-belonging samples drawn from DDIM (Song, Meng, and Ermon 2021), DDGAN (Xiao, Kreis, and Vahdat 2022) and WaveDiff (Phung, Dao, and Tran 2023). We chose CIFAR-10 as it is often used for benchmarking, whereas CelebA-HQ 256 simulates a more realistic scenario with higher resolution and privacy-critical data. For external datasets, we chose them such that they do not strictly belong to the same distribution. That is, CIFAR-10.1 was sampled independently from CIFAR-10, and FFHQ-256 is more diverse than CelebA-HQ 256. This choice is realistic as one cannot assume perfect knowledge of the member distribution, and distribution shifts must be accounted for.⁴

³<https://github.com/tqch/ddpm-torch>

⁴Ideally, they should also be accounted for in our limited member and belonging sets. We focus on external data for simplicity.

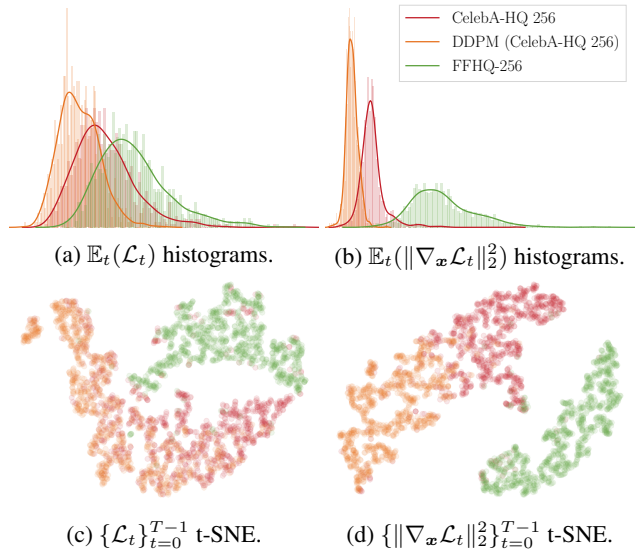


Figure 3: Visualization of CelebA-HQ 256 DDPM features.

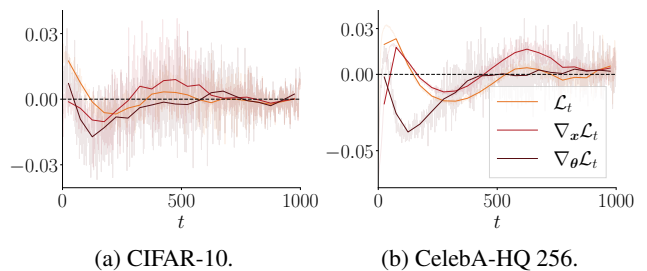


Figure 4: Learned W from (9) for our MIAs. We plot the weights corresponding to different features against t .

Classifier details. Given limited data, we choose a simple architecture, described by (9), for all classifiers to avoid overfitting. We use the AdamW optimizer (Loshchilov and Hutter 2019) and a step learning rate scheduler on the cross entropy loss. Hyperparameters are fixed, shown in Table 1. We normalize features, f , based on training data statistics.

4.2 Analysis

Limitations of threshold-based MIAs. We first conduct experiments that highlight weaknesses of threshold-based MIAs, motivating OA and our trajectory-based attacks.

In Figure 2, we show the sample-averaged \mathcal{L}_t , and, in Figure 3a, we plot histograms of the time-averaged \mathcal{L}_t for different classes of data. Belonging samples attain the lowest values, followed by members and then external samples. Therefore, belonging data falls below the member-external boundary drawn by threshold-based MIAs and is incorrectly classified as member data. This phenomenon is intuitive as the diffusion loss can be seen as a proxy for the negative likelihood (Ho, Jain, and Abbeel 2020) and, by definition, belonging data should achieve the highest likelihoods. We provide further evidence of this by evaluating the MIA of Matsumoto, Miura, and Yanai (2023) in Table 2. Notice that,

Dataset	$t = 50$	$t = 100$	$t = 150$	$t = 200$	$t = 250$	$t = 300$
CIFAR-10	56.3 / 46.4 60.7	60.1 / 44.7 64.3	61.1 / 41.7 66.6	62.2 / 42.8 66.6	62.2 / 42.4 67.3	59.6 / 45.6 65.7
CelebA-HQ 256	64.1 / 48.3 92.4	72.9 / 41.5 94.3	78.9 / 34.2 95.7	83.5 / 31.0 96.5	85.1 / 29.2 96.4	85.9 / 29.2 96.7

Table 2: TPRs / FPRs for MIA using (7). Top values are FPRs on external data, and bottom values are FPRs on belonging data. In the latter case, the TPR, FPR pairs drop below the $y = x$ ROC, making these attacks worse than random guessing.

$t = 0, \dots, 124$	$t = 125, \dots, 249$	$t = 250, \dots, 374$	$t = 375, \dots, 499$	$t = 0, 4, \dots, 496$
68.1	64.5	65.7	63.8	71.6
$t = 0, \dots, 99$	$t = 0, 2, \dots, 198$	$t = 0, 3, \dots, 297$	$t = 0, 4, \dots, 396$	$t = 0, 5, \dots, 495$
66.7	68.7	67.6	69.1	71.3

Table 3: AUC for our loss-based MIAs (member-external) on CIFAR-10. For each row, we fix the number of queries to the DDPM and consider different sampling strategies for t . Global temporal context significantly improves the performance.

when we replace the non-member set with belonging samples in evaluation, the false positives consistently increase.

Besides the issue with belonging data, we observe from Figure 2 that the member-external boundary may not be tight due to distribution shifts. As highlighted by Das, Zhang, and Tramèr (2024), this imperfection can have a significant impact on MIAs. We provide further analysis in Section 4.3.

Global temporal context. Having demonstrated limitations of thresholding, we argue that these methods are insufficient for reliable classification. We next consider multi-step attacks, operating on diffusion trajectories, as described in Section 3.3. Carlini et al. (2023) conjecture that MIAs are most effective when t is restricted to “Goldilocks zone”, i.e., $t \in [50, 300]$. Instead, we hypothesize patterns in the trajectories requiring global temporal context to be revealed.

In Table 3, we show the performance of our MIAs based on different sampling strategies for t with \mathcal{L}_t as features. We find that widely-packed and global features across time are more effective than densely-packed and localized features. This is also corroborated in Figure 4, where we present the learned \mathbf{W} of our classifiers from (9). For clarity, since the weights are noisy, we plot moving averages with solid lines. Notably, the weights are not localized in t , and we observe significant values spanning the majority of the trajectories.

Better features for classification. To better capture the dynamics of diffusion trajectories, we consider adding higher-order gradient features to our classification pipelines.

In Figure 3, we compare histograms and t-SNE (van der Maaten and Hinton 2008) plots for the loss and gradient features collected from our CelebA-HQ 256 model, visualizing 1000 samples from each class. Observe that gradient features are able to separate the three types of data more reliably and are therefore more suitable for classification purposes. Besides, as calculating $\nabla \mathcal{L}_t$ involves calculating \mathcal{L}_t , we can, at no extra cost, construct a richer representation of the trajectories by combining features. We include an ablation study for the features in Table 7 of Appendix A.

4.3 Results

Evaluation metrics. We use Attack Success Rate (ASR), True Positive Rate at 1% False Positive Rate (TPR @ 1% FPR) and Area Under Receiver Operating Characteristic (AUC), since these are commonly adopted in MIA literature.

Comparison partners. As our experiments aim to simulate a realistic attack environment, we will assume minimal data access and no knowledge of the diffusion model training setup. For a fair comparison, we implement the single-time-step MIAs of Matsumoto, Miura, and Yanai (2023), Kong et al. (2024) and the white-box attack of Pang et al. (2024), under the same assumptions and setup, using the recommended settings for each method. Following Das, Zhang, and Tramèr (2024), we also implement model-blind classifiers based on the ResNet18 architecture (He et al. 2016). Specifically, they highlight the importance of distribution shifts in MIAs and show that naive attacks, with no access to the model, may surpass engineered MIAs.

To the best of our knowledge, there are no works on white-box MA or OA for DDPMs. In that case, we report our methods and the model-blind baseline as described above.

Membership inference attacks. We compare MIAs (in the traditional sense, i.e., member and external data) in Table 4. In the CIFAR-10 column, we see that the naive classifier performs slightly better than chance and our setup does not suffer from distribution shifts. However, this baseline performs much better than chance on CelebA-HQ 256. In that case, the threshold-based MIAs of Matsumoto, Miura, and Yanai (2023) and Kong et al. (2024) underperform. Nevertheless, our multi-step approach proves to be robust and remains effective despite the distribution shifts. Additionally, we have the flexibility of trading inference time with performance by adjusting the sampling strategy for t . Specifically, the last two rows in Table 4 show that we maintain competitive performance when reducing our attack times by a factor of three with a coarser, uniform strategy.

Method	CIFAR-10			CelebA-HQ 256					
	AUC	TPR @ 1% FPR	ASR	AUC	TPR @ 1% FPR	ASR			
Naive (model-blind)	52.2	0.0	52.0	94.4	60.1	86.6			
Matsumoto, Miura, and Yanai (2023)	63.2	3.3	59.7	85.2	26.4	76.2			
Kong et al. (2024) (PIA)	66.9	5.1	62.4	62.5	0.1	58.1			
Pang et al. (2024) (GSA ₂)	82.7	12.5	73.5	100.0	99.6	92.5			
Our method									
time-steps	\mathcal{L}_t	$\nabla_x \mathcal{L}_t$	$\nabla_\theta \mathcal{L}_t$						
0, ..., 999	✓			73.3	6.5	68.1	99.1	95.4	96.4
0, 3, ..., 999	✓	✓	✓	81.6	13.4	73.7	100.0	99.9	99.2
0, ..., 999	✓	✓	✓	83.3	16.8	74.8	100.0	100.0	99.5

Table 4: AUC, TPRs @ 1% FPR and ASRs for MIA methods.

Method	CIFAR-10					CelebA-HQ 256									
	DDPM	DDIM	DDGAN	WaveDiff	Overall	DDPM	DDIM	DDGAN	WaveDiff	Overall					
Naive (model-blind)	60.8	39.1	41.9	44.0	51.2	88.3	20.2	22.6	27.0	55.8					
Our method															
time-steps	\mathcal{L}_t	$\nabla \mathcal{L}_t$													
0, ..., 999	✓					75.5	57.6	36.2	64.4	64.1	98.9	6.3	59.6	57.8	70.0
0, 3, ..., 999	✓	✓				86.0	72.4	18.1	76.1	70.8	100.0	7.9	74.2	76.9	76.5
0, ..., 999	✓	✓				87.2	86.8	13.1	91.7	75.5	100.0	3.5	86.8	68.9	76.5

Table 5: Performance of DDPM MA methods. We report per-model and overall (class-balanced) accuracy.

Model attribution. We consider the MA task in Table 5. In particular, given binary classifiers trained with belonging samples from DDPM and non-belonging, real data, we investigate performance on samples that are generated by other models, trained on the same datasets as DDPM. We generate these non-belonging samples from DDIM (Song, Meng, and Ermon 2021), DDGAN (Xiao, Kreis, and Vahdat 2022) and WaveDiff (Phung, Dao, and Tran 2023).

Interestingly, our methods tend to be robust to non-belonging data from other models, whereas the naive method tends to label all synthetic data as belonging. Moreover, combining gradient features improves our classification on DDPM samples and simultaneously enables generalization to other models. However, our method is not without limitations as we are unable to generalize to CIFAR-10 DDGAN and CelebA-HQ 256 DDIM. The relatively high accuracy of the naive approach in these cases is irrelevant as it classifies all synthetic data, regardless of origin, similarly.

Note that the MA algorithm proposed by Wang et al. (2023) does not extend to DDPMs. Specifically, they perform model inversion to obtain the reconstruction loss, which could be uninformative, since perfect reconstruction is always possible from the DDPM latent space (Huberman-Spiegelglas, Kulikov, and Michaeli 2024). In fact, recent work suggests that inversion and reconstruction-based methods in diffusion models may be more suitable for general synthetic image detection (Cazenavette et al. 2024). Besides, as shown in Table 5, by including higher-order features in our pipelines, we outperform the loss by a large margin.

Towards origin attribution. Finally, we are able to combine our methods into one for the three-class OA problem. We present our results for this in Figure 5 and Table 6.

As an application, we use OA as a filter for training data extraction in Figure 6. 30029 belonging images are filtered to 1682. Specifically, we observe that, when our attacks misclassify belonging samples, they consistently assume them to be from the member set. Upon inspection, these misclassified images often resemble members. To quantify such similarities, we use the SSCD⁵ score (Pizzi et al. 2022), following Somepalli et al. (2023); Gu et al. (2024). From Figure 6a, it is clear that similarity is left-skewed for misclassified data, confirming our suspicions.

5 Discussion

We have proposed novel attacks for OA in diffusion models. In this section, we provide discussion on our method, limitations and some directions for future research.

5.1 Comparison With Membership Attacks

Pitfalls of threshold-based MIAs. We showed that traditional attacks for diffusion models (Matsumoto, Miura, and Yanai 2023; Duan et al. 2023; Kong et al. 2024) are intrinsically sub-optimal due to the fact that they cannot handle belonging data. This limitation restricts the scope of membership inference as synthetic data cannot be audited. We also demonstrated that these attacks are not robust to distribution shifts (Das, Zhang, and Tramèr 2024). This may

⁵<https://github.com/facebookresearch/sscd-copy-detection>

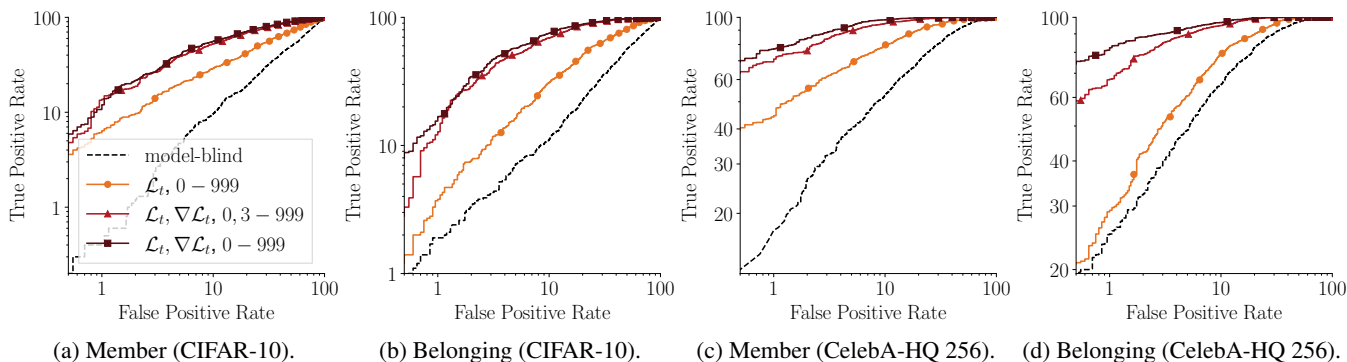
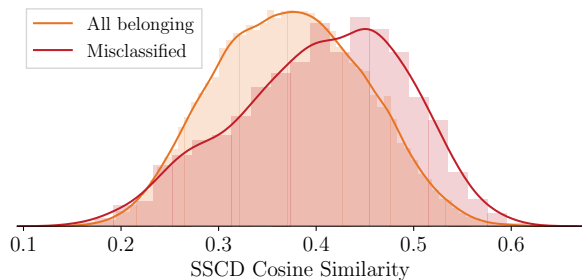


Figure 5: OA ROCs with respect to member and belonging classes.

Method	CIFAR-10			CelebA-HQ 256					
	AUC	TPR @ 1% FPR	ASR	AUC	TPR @ 1% FPR	ASR			
Naive (model-blind)	51.5	1.2	34.7	90.0	32.1	74.4			
Our method									
time-steps	\mathcal{L}_t	$\nabla_x \mathcal{L}_t$	$\nabla_\theta \mathcal{L}_t$						
0, ..., 999	✓			71.6	6.9	54.9	95.2	52.7	84.4
0, 3, ..., 999	✓	✓	✓	85.0	14.3	69.4	98.8	79.5	92.7
0, ..., 999	✓	✓	✓	86.5	15.9	71.1	99.3	86.5	94.1

Table 6: Average AUC, TPRs @ 1% FPR and ASRs for OA methods.



(a) Similarity histograms of belonging images to members.



(b) Misclassified, belonging. (c) Similar members.

Figure 6: We investigate belonging data that is misclassified by our OA algorithm and identify generations suspiciously similar to member data. Similarity is computed with respect to members unseen by the classifier in training.

limit their applicability to artificial environments, where one already assumes knowledge of the member distribution.

Patterns in diffusion trajectories. We then proposed multi-time-step attacks for diffusion models. Our approach is shown to be more robust to distribution shifts and is also extended to OA. Notably, we demonstrated the existence of

patterns in diffusion trajectories that can be leveraged for classification. In contrast to Carlini et al. (2023), who conjecture a "Goldilocks zone" for the time-steps, we showed that it may be beneficial to consider larger time intervals, which could span the entirety of the diffusion process, to uncover global patterns.

5.2 Comparison With Attribution Methods

We address the shortcomings of Wang et al. (2023); Laszkiewicz et al. (2024). In particular, they rely on model or layer inversion techniques, which are not easily adapted for diffusion. To the best of our knowledge, we are the first to demonstrate white-box MA on DDPMs.

5.3 Limitations

Our attacks' times are comparable to DDPM inference. While not unreasonable, this is much slower compared to existing MIAs. Moreover, in MA, we observed failure cases that require further investigation. Given this weakness, our approach to OA could generally be made more robust, especially since our evaluation was on a controlled external set.

5.4 Future Work

A natural next step is the extension of our algorithms to the Stable Diffusion family of models (Rombach et al. 2022). This will require a careful treatment of distribution shifts that may arise due to a highly diversified member set. Another promising direction is employing anomaly detectors with bounded decision areas, as proposed by Laszkiewicz et al. (2024), to improve our methods' performance.

				CIFAR-10			CelebA-HQ 256		
				AUC	TPR @ 1% FPR	ASR	AUC	TPR @ 1% FPR	ASR
PIA	\mathcal{L}_t	$\nabla_x \mathcal{L}_t$	$\nabla_\theta \mathcal{L}_t$	73.3	6.5	68.1	99.1	95.4	96.4
	✓			74.9	6.1	68.5	99.3	97.5	97.3
		✓		77.0	3.1	71.6	100.0	99.5	93.7
	✓	✓	✓	80.0	12.2	72.4	99.7	99.2	98.9
	✓		✓	80.5	10.5	72.8	100.0	99.9	98.4
		✓	✓	81.8	11.1	74.1	100.0	100.0	98.9
	✓	✓	✓	83.3	16.8	74.8	100.0	100.0	99.5
✓	✓			69.5	5.2	64.2	99.2	89.4	95.5
✓		✓		75.6	1.0	68.7	88.1	51.3	80.7
✓			✓	71.7	3.3	64.5	97.1	40.2	92.8
✓	✓	✓		75.3	5.2	68.6	99.3	89.6	95.7
✓	✓		✓	72.9	9.8	66.8	99.2	89.0	96.3
✓		✓	✓	75.6	1.6	68.6	97.5	46.0	93.3
✓	✓	✓	✓	76.3	6.1	69.1	99.3	90.0	96.4

Table 7: Ablation study on the choice of features for our MIAs. We use $t = 0, \dots, 999$ in all experiments.

time-steps	\mathcal{L}_t	$\nabla_x \mathcal{L}_t$	$\nabla_\theta \mathcal{L}_t$	Accuracy
$0, \dots, 999$	✓			26.5
$0, 3, \dots, 999$	✓	✓	✓	31.4
$0, \dots, 999$	✓	✓	✓	31.6

Table 8: CIFAR-10 classification with trajectory features.

References

- Anderson, B. D. 1982. Reverse-time diffusion equation models. *Stochastic Processes and their Applications*, 12(3): 313–326.
- Carlini, N.; Hayes, J.; Nasr, M.; Jagielski, M.; Sehwag, V.; Tramèr, F.; Balle, B.; Ippolito, D.; and Wallace, E. 2023. Extracting training data from diffusion models. In *Proceedings of the 32nd USENIX Conference on Security Symposium, SEC ’23*. USA: USENIX Association. ISBN 978-1-939133-37-3.
- Cazenavette, G.; Sud, A.; Leung, T.; and Usman, B. 2024. Fake-Inversion: Learning to Detect Images from Unseen Models by Inverting Stable Diffusion. *CVPR*.
- Das, D.; Zhang, J.; and Tramèr, F. 2024. Blind Baselines Beat Membership Inference Attacks for Foundation Models. arXiv:2406.16201.
- Dhariwal, P.; and Nichol, A. Q. 2021. Diffusion Models Beat GANs on Image Synthesis. In Beygelzimer, A.; Dauphin, Y.; Liang, P.; and Vaughan, J. W., eds., *Advances in Neural Information Processing Systems*.
- Duan, J.; Kong, F.; Wang, S.; Shi, X.; and Xu, K. 2023. Are diffusion models vulnerable to membership inference attacks? In *Proceedings of the 40th International Conference on Machine Learning, ICML’23*. JMLR.org.
- Dubiński, J.; Kowalczyk, A.; Pawlak, S.; Rokita, P.; Trzciniński, T.; and Morawiecki, P. 2024. Towards More Realistic Membership Inference Attacks on Large Diffusion Models. In *Proceedings of the IEEE/CVF Winter Conference on Applications of Computer Vision (WACV)*, 4860–4869.
- Efron, B. 2011. Tweedie’s Formula and Selection Bias. *Journal of the American Statistical Association*, 106(496): 1602–1614.
- Gu, X.; Du, C.; Pang, T.; Li, C.; Lin, M.; and Wang, Y. 2024. On Memorization in Diffusion Models.
- He, K.; Zhang, X.; Ren, S.; and Sun, J. 2016. Deep Residual Learning for Image Recognition. In *Proceedings of the IEEE Conference on Computer Vision and Pattern Recognition (CVPR)*.
- Ho, J.; Jain, A.; and Abbeel, P. 2020. Denoising Diffusion Probabilistic Models. In Larochelle, H.; Ranzato, M.; Hadsell, R.; Balcan, M.; and Lin, H., eds., *Advances in Neural Information Processing Systems*, volume 33, 6840–6851. Curran Associates, Inc.
- Huberman-Spiegelglas, I.; Kulikov, V.; and Michaeli, T. 2024. An edit friendly DDPM noise space: Inversion and manipulations. In *Proceedings of the IEEE/CVF Conference on Computer Vision and Pattern Recognition*, 12469–12478.
- Karras, T.; Aila, T.; Laine, S.; and Lehtinen, J. 2018. Progressive Growing of GANs for Improved Quality, Stability, and Variation. In *International Conference on Learning Representations*.
- Karras, T.; Aittala, M.; Lehtinen, J.; Hellsten, J.; Aila, T.; and Laine, S. 2024. Analyzing and Improving the Training Dynamics of Diffusion Models. In *Proc. CVPR*.
- Karras, T.; Laine, S.; and Aila, T. 2018. A Style-Based Generator Architecture for Generative Adversarial Networks. *2019 IEEE/CVF Conference on Computer Vision and Pattern Recognition (CVPR)*, 4396–4405.
- Kong, F.; Duan, J.; Ma, R.; Shen, H. T.; Shi, X.; Zhu, X.; and Xu, K. 2024. An Efficient Membership Inference Attack for the Diffusion Model by Proximal Initialization. In

The Twelfth International Conference on Learning Representations.

Krizhevsky, A. 2009. Learning Multiple Layers of Features from Tiny Images.

Laszkiewicz, M.; Ricker, J.; Lederer, J.; and Fischer, A. 2024. Single-Model Attribution of Generative Models Through Final-Layer Inversion. In Salakhutdinov, R.; Kolter, Z.; Heller, K.; Weller, A.; Oliver, N.; Scarlett, J.; and Berkenkamp, F., eds., *Proceedings of the 41st International Conference on Machine Learning*, volume 235 of *Proceedings of Machine Learning Research*, 26007–26042. PMLR.

Loshchilov, I.; and Hutter, F. 2019. Decoupled Weight Decay Regularization. In *International Conference on Learning Representations.*

Ma, R.; Duan, J.; Kong, F.; Shi, X.; and Xu, K. 2023. Exposing the Fake: Effective Diffusion-Generated Images Detection. In *The Second Workshop on New Frontiers in Adversarial Machine Learning.*

Matsumoto, T.; Miura, T.; and Yanai, N. 2023. Membership Inference Attacks against Diffusion Models. In *2023 IEEE Security and Privacy Workshops (SPW)*, 77–83.

Pang, Y.; Wang, T.; Kang, X.; Huai, M.; and Zhang, Y. 2024. White-box Membership Inference Attacks against Diffusion Models. arXiv:2308.06405.

Phung, H.; Dao, Q.; and Tran, A. 2023. Wavelet Diffusion Models Are Fast and Scalable Image Generators. In *Proceedings of the IEEE/CVF Conference on Computer Vision and Pattern Recognition (CVPR)*, 10199–10208.

Pizzi, E.; Roy, S. D.; Ravindra, S. N.; Goyal, P.; and Douze, M. 2022. A Self-Supervised Descriptor for Image Copy Detection. In *2022 IEEE/CVF Conference on Computer Vision and Pattern Recognition (CVPR)*, 14512–14522.

Recht, B.; Roelofs, R.; Schmidt, L.; and Shankar, V. 2018. Do CIFAR-10 Classifiers Generalize to CIFAR-10?

Rombach, R.; Blattmann, A.; Lorenz, D.; Esser, P.; and Ommer, B. 2022. High-Resolution Image Synthesis With Latent Diffusion Models. In *Proceedings of the IEEE/CVF Conference on Computer Vision and Pattern Recognition (CVPR)*, 10684–10695.

Shokri, R.; Stronati, M.; Song, C.; and Shmatikov, V. 2017. Membership Inference Attacks Against Machine Learning Models. In *2017 IEEE Symposium on Security and Privacy (SP)*, 3–18. Los Alamitos, CA, USA: IEEE Computer Society.

Sohl-Dickstein, J.; Weiss, E.; Maheswaranathan, N.; and Ganguli, S. 2015. Deep Unsupervised Learning using Nonequilibrium Thermodynamics. In Bach, F.; and Blei, D., eds., *Proceedings of the 32nd International Conference on Machine Learning*, volume 37 of *Proceedings of Machine Learning Research*, 2256–2265. Lille, France: PMLR.

Somepalli, G.; Singla, V.; Goldblum, M.; Geiping, J.; and Goldstein, T. 2023. Diffusion Art or Digital Forgery? Investigating Data Replication in Diffusion Models. In *2023 IEEE/CVF Conference on Computer Vision and Pattern Recognition (CVPR)*, 6048–6058.

Song, J.; Meng, C.; and Ermon, S. 2021. Denoising Diffusion Implicit Models. In *International Conference on Learning Representations.*

Song, Y.; Sohl-Dickstein, J.; Kingma, D. P.; Kumar, A.; Ermon, S.; and Poole, B. 2021. Score-Based Generative Modeling through Stochastic Differential Equations. In *International Conference on Learning Representations.*

Torralba, A.; Fergus, R.; and Freeman, W. T. 2008. 80 Million Tiny Images: A Large Data Set for Nonparametric Object and Scene Recognition. *IEEE Transactions on Pattern Analysis and Machine Intelligence*, 30(11): 1958–1970.

van der Maaten, L.; and Hinton, G. 2008. Visualizing Data using t-SNE. *Journal of Machine Learning Research*, 9(86): 2579–2605.

Wang, Z.; Chen, C.; Lyu, L.; Metaxas, D. N.; and Ma, S. 2024. DIAGNOSIS: Detecting Unauthorized Data Usages in Text-to-image Diffusion Models. In *The Twelfth International Conference on Learning Representations.*

Wang, Z.; Chen, C.; Zeng, Y.; Lyu, L.; and Ma, S. 2023. Where Did I Come From? Origin Attribution of AI-Generated Images. In *Thirty-seventh Conference on Neural Information Processing Systems.*

Wen, Y.; Liu, Y.; Chen, C.; and Lyu, L. 2024. Detecting, Explaining, and Mitigating Memorization in Diffusion Models. In *The Twelfth International Conference on Learning Representations.*

Xiao, Z.; Kreis, K.; and Vahdat, A. 2022. Tackling the Generative Learning Trilemma with Denoising Diffusion GANs. In *International Conference on Learning Representations.*

Yeom, S.; Giacomelli, I.; Fredrikson, M.; and Jha, S. 2018. Privacy Risk in Machine Learning: Analyzing the Connection to Overfitting. In *2018 IEEE 31st Computer Security Foundations Symposium (CSF)*, 268–282. Los Alamitos, CA, USA: IEEE Computer Society.

A The Choice of Features

We experiment with different features for modeling the diffusion trajectories in Table 7. PIA from Kong et al. (2024) is also adapted and integrated with our methods. Specifically, when using PIA, we replace $\epsilon \sim \mathcal{N}(\mathbf{0}, \mathbf{I})$ in \mathcal{L}_t with $\epsilon_\theta(\mathbf{x}, 0)$, which makes the trajectory features deterministic.

From Table 7, we see that all features are capable of separating the data individually. When combined, the performance is significantly increased, and this leads our proposed algorithm. Note that the PIA features are not as robust as their stochastic counterparts. We hypothesize that the added stochasticity is helpful in this case as it acts as a regularizer.

B Trajectory-Based CIFAR-10 Classifier

We investigate whether trajectories can reveal the class of samples on CIFAR-10 in Table 8. We pick a class-balanced dataset of 1000 samples from the member set for classifier training and evaluate on another similarly chosen dataset.

Interestingly, we find that trajectory-based classification performs much better than random guessing ($\sim 10\%$), and this strengthens our argument for the existence of hidden patterns in diffusion trajectories.